

Fifteen-Year Global Time Series of Satellite-Derived Fine Particulate Matter

B. L. Boys,^{*†} R. V. Martin,^{†,‡} A. van Donkelaar,[†] R. J. MacDonell,[†] N. C. Hsu,[§] M. J. Cooper,[†] R. M. Yantosca,^{||} Z. Lu,[†] D. G. Streets,[†] Q. Zhang,[#] and S. W. Wang[#]

[†]Dalhousie University, Halifax, Nova Scotia Canada

[‡]Harvard-Smithsonian Center for Astrophysics, Cambridge, Massachusetts 02138, United States

[§]NASA Goddard Space Flight Center, Greenbelt, Maryland 20771, United States

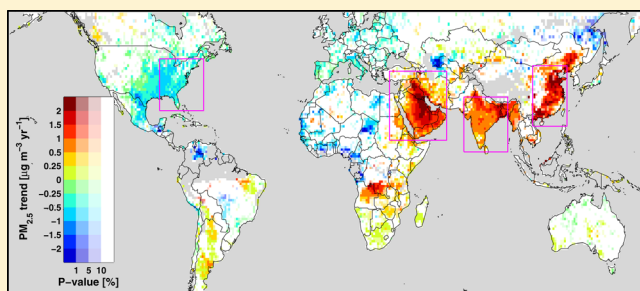
^{||}Harvard University, Cambridge, Massachusetts 02138, United States

[†]Argonne National Laboratory, Argonne, Illinois 60439, United States

[#]Center for Earth System Science, Tsinghua University, Beijing, China

S Supporting Information

ABSTRACT: Ambient fine particulate matter ($\text{PM}_{2.5}$) is a leading environmental risk factor for premature mortality. We use aerosol optical depth (AOD) retrieved from two satellite instruments, MISR and SeaWiFS, to produce a unified 15-year global time series (1998–2012) of ground-level $\text{PM}_{2.5}$ concentration at a resolution of $1^\circ \times 1^\circ$. The GEOS-Chem chemical transport model (CTM) is used to relate each individual AOD retrieval to ground-level $\text{PM}_{2.5}$. Four broad areas showing significant, spatially coherent, annual trends are examined in detail: the Eastern U.S. ($-0.39 \pm 0.10 \mu\text{g m}^{-3} \text{ yr}^{-1}$), the Arabian Peninsula ($0.81 \pm 0.21 \mu\text{g m}^{-3} \text{ yr}^{-1}$), South Asia ($0.93 \pm 0.22 \mu\text{g m}^{-3} \text{ yr}^{-1}$) and East Asia ($0.79 \pm 0.27 \mu\text{g m}^{-3} \text{ yr}^{-1}$). Over the period of dense in situ observation (1999–2012), the linear tendency for the Eastern U.S. ($-0.37 \pm 0.13 \mu\text{g m}^{-3} \text{ yr}^{-1}$) agrees well with that from in situ measurements ($-0.38 \pm 0.06 \mu\text{g m}^{-3} \text{ yr}^{-1}$). A GEOS-Chem simulation reveals that secondary inorganic aerosols largely explain the observed $\text{PM}_{2.5}$ trend over the Eastern U.S., South Asia, and East Asia, while mineral dust largely explains the observed trend over the Arabian Peninsula.



INTRODUCTION

Particles with an aerodynamic diameter below $2.5 \mu\text{m}$ ($\text{PM}_{2.5}$) are highly respirable and are a leading global environmental risk factor for premature mortality.^{1–4} Recently, the World Health Organization (WHO) declared particulate matter air pollution a group 1 carcinogen to humans,⁵ adding to the known burden of disease from cardiovascular and respiratory morbidity. The WHO air quality guideline (AQG) for $\text{PM}_{2.5}$ of $10 \mu\text{g m}^{-3}$ is surpassed in most industrialized regions of the world, in some areas by an order of magnitude.⁶ In addition to the detrimental health effects of elevated $\text{PM}_{2.5}$ concentrations, epidemiological research of 545 U.S. counties² and a Canadian national-level cohort⁷ failed to identify an exposure threshold where $\text{PM}_{2.5}$ reductions provided no benefit. A recent study points to prenatal morbidity at levels below the present European Union annual limit of $25 \mu\text{g m}^{-3}$.⁴ Long-term time series of spatially resolved $\text{PM}_{2.5}$ on the global scale are needed to assess health impacts and inform policy decisions.

Satellite-derived estimates of ground-level $\text{PM}_{2.5}$ have advanced in recent years due to the developments of advanced column aerosol optical depth (AOD) satellite retrievals, of global chemical transport models (CTMs) and of ground-level

in situ observations of $\text{PM}_{2.5}$.⁸ Satellite-retrieved AOD, a unitless measure of the column-integrated extinction of radiation by atmospheric particles, can be related to surface $\text{PM}_{2.5}$ by [1] use of a chemical transport model to simulate daily the $\text{PM}_{2.5}$ to AOD relationship^{6,9} and by [2] statistical methods where reliable monitoring networks are used as a training data set to calibrate daily $\text{PM}_{2.5}$ to AOD relationships.^{10,11} The latter method can provide highly accurate $\text{PM}_{2.5}$ to AOD relationships in regions with a sufficiently dense network of ground-level measurements, while the former method can be validated where ground measurements exist and then applied beyond the reach of globally sparse measurement networks. The surface $\text{PM}_{2.5}$ to column AOD relationship has substantial seasonal variability and daily fluctuations.¹¹ Interannual variations in this relationship from changing emissions and meteorological fluctuations could complicate comparison of AOD and $\text{PM}_{2.5}$ trends such that a

Received: April 29, 2014

Revised: August 22, 2014

Accepted: September 3, 2014

Published: September 3, 2014

significant trend in AOD may not necessarily manifest as a significant trend in PM_{2.5} and vice versa. Accordingly, methods to estimate spatiotemporally resolved global PM_{2.5} to AOD ratios are a requirement for accurate study of the trend in satellite-derived PM_{2.5}.

Satellite-retrieved AOD is subject to a suite of uncertainties with contributions from sampling bias, cloud contamination, assumptions of aerosol and surface properties, and erroneous sensor calibration.^{12,13} Radiometric stability is of particular importance to time series analysis; spurious trends in long-term AOD have been inferred as a result of radiometric drift.^{14,15} Unfortunately, both of the Moderate Resolution Imaging Spectroradiometer (MODIS) sensors onboard NASA's Terra and Aqua satellites exhibit radiometric drift in the collection 5 product,¹⁵ an issue that is addressed in the recent collection 6 product.¹⁶ The sea-viewing wide field-of-view sensor (SeaWiFS), the sole instrument on board NASA's SeaStar satellite, was designed primarily for global ocean color measurement and thus required highly accurate calibration that was maintained to an accuracy of 0.5% with stability of 0.3%.^{17,18} The multiangle imaging spectroradiometer (MISR) onboard NASA's Terra satellite, an advanced earth observing sensor designed primarily to retrieve tropospheric aerosol properties, is maintained to an accuracy of 3% with stability of 1%.^{19,20} Decadal variations in satellite-retrieved AOD from SeaWiFS and MISR have been examined globally and evaluated with NASA's ground-based Aerosol Robotic Network (AERONET) of sunphotometers.^{15,21–23}

Globally, few regional scale PM_{2.5} trends have been inferred from in situ measurements due to a lack of long-term monitoring networks. However, in the U.S., sufficient measurements have enabled detection of a 33% decrease in PM_{2.5} from 2000 to 2012, with most measurement sites located in the Eastern U.S. (<http://www.epa.gov/airtrends/>). Visibility, a widely used measure of near surface extinction by aerosol, has decreased globally over land during the past few decades, with industrializing regions such as South and East Asia experiencing the greatest declines.²⁴ This is in contrast with improvements seen for postindustrialized Europe from the late 1980s to 2000, a result of large reductions in sulfate aerosol over this period.²⁵ Efforts to improve air quality have resulted in decreases in particulate matter with diameter <10 μm (PM₁₀) over North America, Europe and more recently East Asia.^{26,27} However, due to the low extinction efficiency of visible radiation by these coarse particles, decreasing trends in PM₁₀ are not necessarily matched with improvements in visibility, especially in industrializing nations such as East Asia where the ratio of fine to coarse particles has increased.²⁷ Regional analysis of satellite-derived PM_{2.5} at 0.5° × 0.5° over the Indian subcontinent using the MISR time series from 2000 to 2010 and climatological "surface PM_{2.5} to column AOD" relationships revealed an increase of 15 to >25 μg m⁻³ over the Indo-Gangetic Basin, with increases for central India in the range 5–15 μg m⁻³.²⁸ Hu et al.¹⁰ detected a 20% decrease in PM_{2.5} over 2001 to 2010 for the southeastern U.S., with greater reductions observed for urban and highway environments than for more remote forest areas.

In this study, we develop and interpret the first observationally based estimate of changes in long-term global PM_{2.5}. Specifically, we combine satellite-derived PM_{2.5} from the MISR and SeaWiFS instruments—using overpass-resolved simulated 'surface PM_{2.5} to column AOD' relationships from a global CTM employing consistent assimilated meteorology—

to estimate and interpret a unified, 24 h, monthly PM_{2.5} time series from January 1998 to December 2012 globally at a resolution of 1° × 1° which is amenable to time series analysis. Significant annual trends observed over four broad regions, namely: Eastern U.S., Arabian Peninsula, South Asia, and East Asia, are analyzed together with simulated PM_{2.5} fractional components.

MATERIALS AND METHODS

Retrieved Satellite Aerosol Optical Depth. MISR contains nine fixed angle cameras, enabling sensitivity to angular variation in reflected sunlight originating from aerosols, clouds and surface. This allows retrieval of aerosol properties with reduced algorithmic assumptions of surface reflectance over all land types,^{29,30} including terrain with temporally varying surface features and highly reflective surfaces like deserts.³¹ AOD is retrieved from MISR at a resolution of 17.6 × 17.6 km. The equator crossing time is 1030 h local solar time. The 360 km across track swath results in global coverage in 9 days at the equator and 2 days near the poles. We regridded to daily 1° × 1° global AOD maps from 29 February 2000 to 31 December 2012, using daily level 2 AOD swaths at 558 nm (from the MIL2ASAE product with quality assurance flags [0 1]).

The visible to near IR spectral range of SeaWiFS allows AOD retrieval algorithms to be applied over both ocean³² and land,³³ yielding accuracies similar to other AOD retrieving satellites.³⁴ SeaWiFS retrievals of AOD are at a resolution of 13.5 × 13.5 km with an equator crossing time of 1200 h local solar time, drifting to ca. 1430 h by 2010. A 1502 km across track swath results in near daily coverage at the equator and daily coverage outside the tropics. We regridded to daily 1° × 1° global AOD maps from 01 January 1998 to mission end date December 2010, using daily level 2 AOD swaths at 550 nm (version SWDB_L2.004 with quality assurance [2 3] over ocean and [3] over land).

Satellite-Derived PM_{2.5}. Following van Donkelaar et al. 2010⁶ we expressed the proportionality between ground-level PM_{2.5} mass concentration and satellite-retrieved column-integrated AOD as spatially and temporally resolved correction factors [η]:

$$\text{PM}_{2.5} = \eta \times \text{AOD}, \quad \eta = \frac{\text{PM}_{2.5}^{\text{model}}}{\text{AOD}^{\text{model}}} \quad (1)$$

where η [μg m⁻³] is the ratio of modeled PM_{2.5} [μg m⁻³] under reference conditions to modeled column-integrated AOD [unitless] under ambient relative humidity. We used the North American surface measurement standard of 35% relative humidity³⁵ to reference our PM_{2.5} estimates. Factors which influence the value of η include [1] the vertical distribution of the aerosol burden, [2] the aerosol size distribution, [3] aerosol composition, and [4] relative humidity. We calculated daily global maps of η with the 3-D global CTM, GEOS-Chem [geos-chem.org; supplemental] for the period 1 January 1998 to 31 December 2012. The relation of satellite AOD to PM_{2.5} is enabled because the aerosol mass extinction efficiency for visible radiation happens to peak within the accumulation mode (~0.1 to 2.5 μm diameter particles) of the aerosol size distribution, which is the size region contributing to PM_{2.5}.

GEOS-Chem^{36,37} solves for the 3-D evolution of atmospheric gases and aerosols (sulfate, nitrate, ammonium, organic and black carbon, mineral dust, and sea salt) using assimilated

meteorological observations, global and regional emission inventories, and algorithms to represent the physics and chemistry of atmospheric processes, as described in the Supporting Information (SI). The CTM was driven by assimilated meteorological observations (GEOS-MERRA) at a horizontal resolution of $2^\circ \times 2.5^\circ$ (lat, long) with 47 vertical levels from the surface to ca. 80 km. Modeled PM_{2.5} and column AOD used in the formulation of η were sampled at satellite overpass time (late morning for MISR and early afternoon for SeaWiFS). Daily global maps of η at $2^\circ \times 2.5^\circ$ were interpolated to $1^\circ \times 1^\circ$ for application to satellite AOD values. Following van Donkelaar et al. 2013,³⁸ for absolute satellite-derived PM_{2.5} estimates, we scaled the vertical distribution of modeled aerosol extinction to match climatological monthly observations from the CALIPSO satellite lidar at $1^\circ \times 1^\circ$ over 2006–2012. However, our analysis of time varying PM_{2.5} anomalies does not employ such correction factors since CALIPSO was not operational prior to 2006.

Combined Satellite-Derived PM_{2.5}. A unified, monthly, satellite-derived PM_{2.5} global time series at $1^\circ \times 1^\circ$ from 1 January 1998 to 31 December 2012 was estimated by combining the sampling-corrected (SC), monthly SeaWiFS (1998–2010) and MISR (2000–2012) derived PM_{2.5} time series. We accounted for sampling differences as

$$\text{SC_MISR_PM}_{2.5,m} = \frac{\text{GC_PM}_{2.5,m}^{24\text{ h}}}{\text{GC_PM}_{2.5,m}^{\text{MISR}}} \times \text{MISR_PM}_{2.5,m} \quad (2)$$

$$\text{SC_SeaWiFS_PM}_{2.5,m} = \frac{\text{GC_PM}_{2.5,m}^{24\text{ h}}}{\text{GC_PM}_{2.5,m}^{\text{SeaWiFS}}} \times \text{SeaWiFS_PM}_{2.5,m} \quad (3)$$

where, for month m , MISR_{PM}_{2.5,m} and SeaWiFS_{PM}_{2.5,m} refer to monthly satellite-derived PM_{2.5} estimates from respective instruments—a threshold of at least 3 days per month for each $1^\circ \times 1^\circ$ grid cell was required for monthly PM_{2.5} averages. GC_{PM}_{2.5,m}^{24 h} refers to monthly mean GEOS-Chem PM_{2.5} averaged over 24 h for each day of the month. GC_{PM}_{2.5,m}^{SeaWiFS} and GC_{PM}_{2.5,m}^{MISR} refer to monthly mean GEOS-Chem PM_{2.5} sampled on coincident days with each instrument during the corresponding satellite overpass period (i.e., late morning for MISR, early afternoon for SeaWiFS). Monthly modeled correction factors for incomplete sampling display distinct seasonality, as in van Donkelaar et al. 2010,⁶ especially for regions with pronounced wet and dry seasons (data not shown).

When monthly averages for each sensor exist, we calculated PM_{2.5,m} as the average of monthly mean satellite-derived PM_{2.5} from each instrument after accounting for their sampling differences (as shown in 2 and 3);

$$\text{PM}_{2.5,m} = \frac{1}{2} \text{SC_MISR_PM}_{2.5,m} + \frac{1}{2} \text{SC_SeaWiFS_PM}_{2.5,m} \quad (4)$$

When just one of the two satellite sensors had sufficient data to represent a monthly average, or during a pre- or postperiod of operation, a virtual estimate of the sampling-corrected missing value (i.e., SC_{MISR}_{PM}_{2.5,m}^{vir}) was computed [5] and used in [4].

$$\begin{aligned} & \text{SC_MISR_PM}_{2.5,m}^{\text{vir}} \\ &= \left(\frac{1}{8} \sum_{y=2001}^{2008} \text{SC_MISR_PM}_{2.5,m(y)}^{\text{offset}} \right) \\ &\quad \times \text{SC_SeaWiFS_PM}_{2.5,m} \end{aligned} \quad (5)$$

where, for month m , $(1/8 \sum_{y=2001}^{2008} \text{SC_MISR_PM}_{2.5,m(y)}^{\text{offset}})$ is the month-specific, sampling-corrected climatological offset for MISR, and SC_{SeaWiFS}_{PM}_{2.5,m} is the sampling-corrected estimate of SeaWiFS-derived PM_{2.5}. Month-specific climatological offset factors for MISR and SeaWiFS were computed using the years y from 2001 to 2008, an overlap period of optimal performance for both sensors. Similar methods have been used to estimate daytime PM_{2.5} over United States New England region by averaging MODIS-Terra (1030 h overpass) and MODIS-Aqua (1330 h overpass) values.³⁹ We assessed the sensitivity of trends over the four regions examined herein to uncertainty in offset by compiling 15 combined satellite-derived PM_{2.5} time series where for each year an offset value was drawn at random from a normal distribution described by mean and variance inferred between 2001 and 2008. The 1σ standard deviation inferred from resulting trends was found to be within 27% of corresponding trends for all four regions.

We interpreted the satellite-derived PM_{2.5} time series with the GEOS-Chem model. We expressed the satellite-derived monthly PM_{2.5} concentration attributable to each major chemical component (secondary inorganics \equiv sulfate + nitrate + ammonium, carbonaceous \equiv organic + black carbon, mineral dust, and sea salt) as the satellite-derived concentration scaled by the GEOS-Chem fractional concentration for each component.

In Situ PM_{2.5}. We evaluated the satellite-derived PM_{2.5} time series anomaly with ground-based PM_{2.5} measurements in the Eastern U.S. (east of 90°W) where there is a sufficiently dense, long-term federal reference method (FRM) data record from the Interagency Monitoring of Protected Visual Environments network (IMPROVE; <http://vista.cira.colostate.edu/improve/>) and from the Environmental Protection Agency Air Quality System (EPA AQ; <http://www.epa.gov/ttn/airs/airsaqs/>). U.S. FRM 24 h gravimetric filter based in situ measurements (PM_{2.5}—local conditions, selections from parameter code 88101) were obtained for years 1998 through 2012 (<http://www.epa.gov/ttn/airs/airsaqs/detailldata/downloadaqsdata.htm>). For comparison to satellite-derived PM_{2.5}, daily in situ measurements were spatially aggregated first to a daily $1^\circ \times 1^\circ$ grid, followed by temporal averaging to a monthly $1^\circ \times 1^\circ$ grid, followed by spatial averaging for regional analysis; an approach analogous to satellite-derived PM_{2.5} since space-time averaging is not commutative for discontinuous data sets.⁴⁰ We focus our evaluation on the long-term trend since that is the emphasis of this study.

Estimated PM_{2.5} to AOD Relationship from In Situ PM_{2.5} and AERONET AOD over the Eastern U.S. We evaluated the modeled PM_{2.5} to AOD monthly time series with and without the use of monthly CALIPSO-based correction factors, by comparison with empirical estimates from ground-based measurements over the Eastern U.S. (east of 90°W). Monthly estimates of the PM_{2.5} to AOD relationship from January 1998 to December 2012 were compiled by aggregating daily AERONET Level 2 AOD measurements (<http://aeronet.gsfc.nasa.gov/>) from 1000 to 1400 h with coincident, at $1^\circ \times 1^\circ$, daily U.S. FRM 24 h gravimetric filter-based in situ

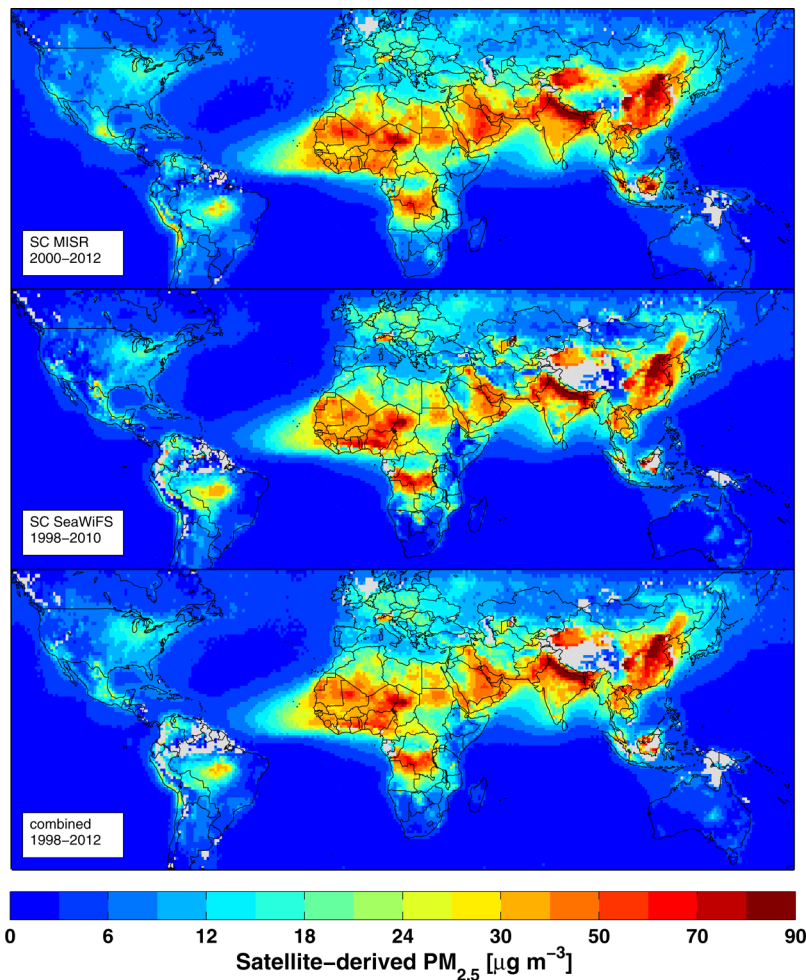


Figure 1. Satellite-derived, 24 h, sampling-corrected PM_{2.5} from MISR averaged over 2000–2012, SeaWiFS averaged over 1998–2010, and a combined MISR-SeaWiFS product averaged over 1998–2012. Gray indicates missing data.

measurements. AERONET and PM_{2.5} stations with an elevation difference of more than 100 m were excluded.

Time Series Analysis. Time series analysis was performed on data aggregated to monthly arithmetic mean values. General Least Squares (GLS) regression was performed using the basic model:

$$\mathbf{x} = \mathbf{z}\boldsymbol{\beta} + \mathbf{e}, \quad \mathbf{e} \sim N(0, \sigma^2 \mathbf{V}) \quad (4)$$

where for a time series of n months, \mathbf{x} is a time series vector ($n \times 1$) containing PM_{2.5} values for months 1 to n ; \mathbf{z} is a design matrix ($n \times 2$) which herein defines a linear model; $\boldsymbol{\beta}$ is a vector (2×1) containing the coefficients of the linear model, intercept and slope; \mathbf{e} is an error vector ($n \times 1$) containing the residuals not represented by the linear model, which for validity should be approximately normally distributed with zero mean, however, permitted to covary with adjacent values according to \mathbf{V} —a positive definite, symmetric covariance matrix, to accommodate possible autocorrelation between adjacent months. Correlated errors between adjacent months are represented by a first order autoregressive model of \mathbf{e} , which can be expressed as

$$\mathbf{e}_m = \phi \mathbf{e}_{m-1} + \mathbf{w}_m, \quad m = 1, \dots, n, \quad \mathbf{w} \sim N(0, \sigma^2 \mathbf{I}) \quad (5)$$

where the residual \mathbf{e}_m for month m is a fraction ϕ of the previous month's residual \mathbf{e}_{m-1} with a white noise component \mathbf{w}_m , which for validity should be approximately normally

distributed with zero mean, constant variance and independent. Such linear models are widely used in the analysis of environmental monthly time series data.^{41–43} The monthly time series was deseasonalized by subtracting the climatological monthly median prior to GLS regression. A minimum temporal coverage of 65% was applied to all $1^\circ \times 1^\circ$ time series prior to spatial averaging for regional analysis to ensure annual representation of regional trends.

RESULTS AND DISCUSSION

Figure 1 shows global distributions of multiyear average, satellite-derived, ground-level PM_{2.5} at $1^\circ \times 1^\circ$. The data for sampling-corrected MISR over 2000–2012 and for sampling-corrected SeaWiFS over 1998–2010 exhibit a high degree of consistency despite having very different retrieval algorithms and slight differences in periods of observation. Both indicate broad enhancements across North Africa, the Middle East, South Asia, and East Asia. Inspection of coincidently sampled MISR- and SeaWiFS-derived climatologies reveals regions of notable difference affected by sampling, such as the biomass burning feature of South America and SeaWiFS lows over the Appalachian Mountains and Tibetan Plateau. Remaining areas of difference, namely, central India and the western Arabian Peninsula, arise from differing instrument and retrieval characteristics.³⁴ SI Figure S1 (top panel) depicts the percent difference between sampling-corrected MISR- and sampling-

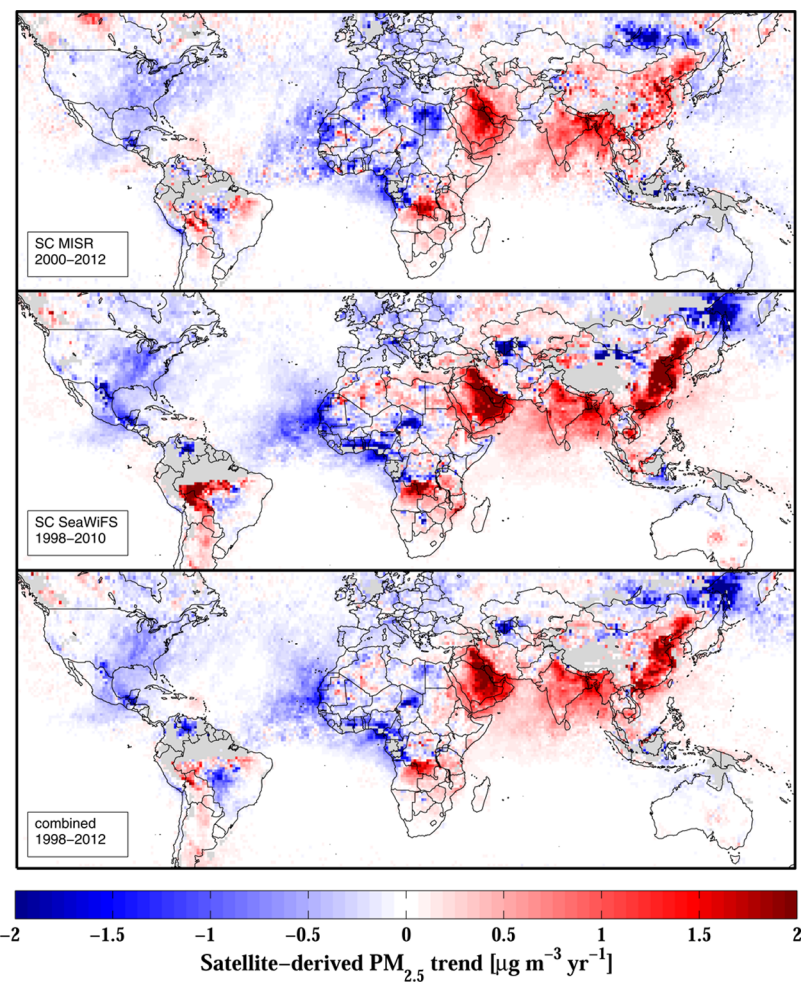


Figure 2. Slope from linear regression of satellite-derived, 24 h, sampling-corrected, monthly PM_{2.5} time series from MISR over 2000–2012, SeaWiFS over 1998–2010, and a combined MISR-SeaWiFS product over 1998–2012. Gray indicates missing data.

corrected SeaWiFS-derived PM_{2.5} climatologies for overlapping years 2000–2010, which indicates the importance of accounting for climatological offsets when combining the two time series. The MISR-SeaWiFS combined product increases the number of observations and reduces instrument-specific bias through averaging to produce a more representative PM_{2.5} concentration map.

Figure 2 shows global maps of the linear trend through satellite-derived PM_{2.5} monthly mean time series. SI Figure S2 depicts the fraction of months included in the time series. Five regions exhibit spatially broad correlation between MISR- and SeaWiFS-derived trend maps: Eastern U.S., Central Europe, the Arabian Peninsula, South Asia, and East Asia. The combined time series preserves these spatial tendencies. Regions of notable difference between MISR- and SeaWiFS-derived trend maps resulting from features missed by one instrument due to different periods of observation include the decreasing SeaWiFS trend over Eastern Russia due to intense wildfires during summer of 1998,⁴⁴ the increasing SeaWiFS trend over the biomass burning area of South America which exhibits a sharp decline in 2006⁴⁵ and again after 2010, and the decreasing dust-driven SeaWiFS trend west of the Sahara. The absence of a spatially coherent trend over the remote subtropical southern ocean, as expected for this region, provides confidence in instrument stability.⁴⁶ Some of these differences partially arise from remaining diurnal sampling differences and instrument-

specific AOD retrieval bias as seen in trend maps created for overlapping years 2000–2010 (SI Figure S1).

SI Figure S3 shows contributions from interannual variations in modeled η (surface PM_{2.5} to column AOD) depicted as linear tendencies. Trends in η can strengthen PM_{2.5} trends compared to AOD trends in regions of changing surface emissions, such as the Eastern U.S. or China as seen in the bottom panel by comparing trends in modeled η to those inferred from a simulation using constant anthropogenic emissions. Or trends in η can dampen PM_{2.5} trends compared to AOD trends for regions with significant change in the vertical aerosol distribution, such as locations with a stable boundary layer downwind of strong lofted sources (i.e., Pacific Ocean west of Peru). Note that trends in surface PM_{2.5} cannot be interpreted from trends in η prior to scaling such trends by AOD.

We evaluated the simulated change in η over the Eastern U.S., a region with the densest collection of PM_{2.5} and AERONET measurements over 1999–2012 allowing coincidentally (daily) sampled monthly time series of five 1° × 1° grid cells with a minimum of 65% temporal coverage. Significant decreasing tendencies in η are found over the Eastern U.S. in both empirical estimates ($-1.9 \pm 0.8 \mu\text{g m}^{-3} \text{ yr}^{-1}$) and coincidentally sampled modeled ($-0.9 \pm 0.5 \mu\text{g m}^{-3} \text{ yr}^{-1}$) monthly time series over 1999–2012. This empirical trend in η emphasizes the need to account for interannual variation in η .

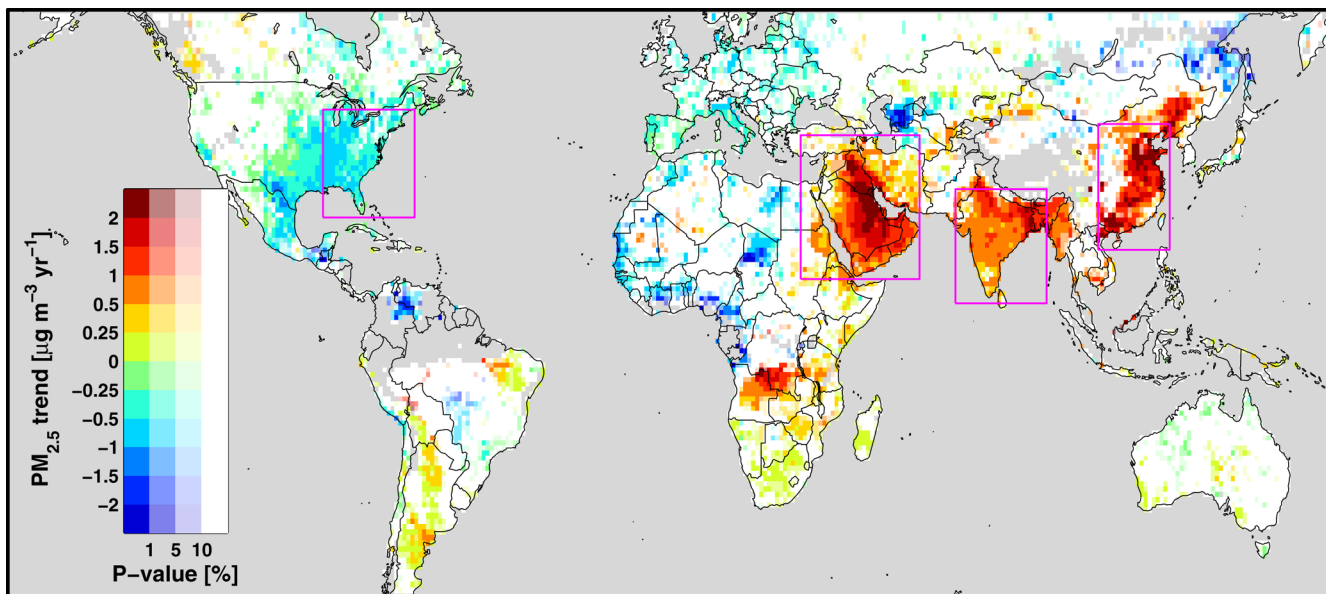


Figure 3. Statistical significance of the trend inferred from linear regression of monthly PM_{2.5} time series inferred from the MISR-SeaWiFS combined product over 1998–2012. Magenta boxes indicate areas featured for regional analysis. Gray indicates water or missing data.

for satellite-derived time series of PM_{2.5}. Applying climatological (2006–2011) month-specific CALIPSO scale factors to adjust the simulation of η over 1999–2012 would degrade the modeled trend in η ($-0.2 \pm 0.4 \mu\text{g m}^{-3} \text{yr}^{-1}$) and accordingly worsen comparisons of satellite-derived and in situ PM_{2.5} trends over the Eastern U.S.; this is likely a result of CALIPSO observations being available only in the second half of the time series.

Figure 3 shows the statistical significance of the combined PM_{2.5} trend over land in the form of a two sided P-value, tested against null being zero trend. Four broad regions with notable significant PM_{2.5} tendencies over the 15-years of study are indicated and discussed below. Other smaller areas of significant tendency include the Po Valley of Italy,²² and the west coast of Africa.²¹ The strong negative tendency appearing over the Aral Sea area may arise from an artifact in part of the SeaWiFS AOD time series for this region as consequence of surface assumptions over a changing bright surface; the MISR time series shows no such feature as MISR simultaneously retrieves surface reflectance along with AOD.

Figure 4 shows the regional monthly time series anomaly for the four areas highlighted in Figure 3: Eastern U.S., the Arabian Peninsula, South Asia, and East Asia. Black lines indicate regional monthly anomalies from the combined PM_{2.5} time series and corresponding linear fit. Colored lines depict the satellite-derived PM_{2.5} trend attributable to modeled PM_{2.5} components. Table 1 contains, for all four regions, numerical values of trends in satellite-derived PM_{2.5} and in model attributed PM_{2.5} components. The in situ PM_{2.5} trend is included for the Eastern U.S. SI Figure S4 depicts the four regional time series on an absolute scale with simulated PM_{2.5} concentrations included for comparison. Trends in SI Figure S4 are likely less accurate than in Figure 4 due to the use of CALIPSO measurements taken during only part of the time series. Below we discuss each region in detail.

Eastern United States. The spatially broad and significant decreasing tendencies found in satellite-derived PM_{2.5} for the Eastern U.S. are well supported by a dense network of ground-based in situ measurements (SI Figure S5). As shown in Table

1, the 1998–2012 linear tendency for this region of $-0.39 \pm 0.10 \mu\text{g m}^{-3} \text{yr}^{-1}$ for the satellite-derived combined time series becomes $-0.37 \pm 0.13 \mu\text{g m}^{-3} \text{yr}^{-1}$ over the period of in situ observations (1999–2012) and is consistent with the in situ trend ($-0.38 \pm 0.06 \mu\text{g m}^{-3} \text{yr}^{-1}$). The in situ trend over the Eastern U.S. was inferred from ca. $380 1^\circ \times 1^\circ$ grid cells, yielding nearly complete spatial coverage of this region at this resolution, with an average of 1.9 in situ stations per cell (SI Figure S5). Excluding in situ stations with “urban” designation reduces spatial coverage to ca. $260 1^\circ \times 1^\circ$ grid cells with an average of 1.5 in situ stations per cell, however, affects neither trend inferred from in situ measurements nor combined satellite product within the bounds of 95% CI. Agreement is also observed when monthly values are aggregated from median (in situ: $-0.34 \pm 0.05 \mu\text{g m}^{-3} \text{yr}^{-1}$, combined satellite: $-0.33 \pm 0.11 \mu\text{g m}^{-3} \text{yr}^{-1}$) and geometric (in situ: $-0.33 \pm 0.04 \mu\text{g m}^{-3} \text{yr}^{-1}$, combined satellite: $-0.32 \pm 0.11 \mu\text{g m}^{-3} \text{yr}^{-1}$) averages. The GEOS-Chem simulation attributes the trend in the Eastern U.S. almost entirely to secondary inorganic aerosols (Figure 4), similar to the findings of Leibensperger et al.⁴⁷ Careful inspection of the satellite-derived PM_{2.5} time series anomaly in Figure 4 reveals three distinct sections which mirror U.S. emissions of sulfur dioxide (<http://www.epa.gov/air/airtrends/sulfur.html>): [1] 1998–2002 a period of decreasing tendency, [2] 2002–2006 a period of stability, [3] 2006–2012 a period of decreasing tendency. The comparison to the in situ trend for this region is degraded when either η is treated as a constant ($-0.22 \pm 0.09 \mu\text{g m}^{-3} \text{yr}^{-1}$) or CALIPSO-adjusted η values are employed ($-0.24 \pm 0.08 \mu\text{g m}^{-3} \text{yr}^{-1}$). The larger uncertainty range of the satellite-derived combined time series ($\pm 0.13 \mu\text{g m}^{-3} \text{yr}^{-1}$) compared to that for in situ observations ($\pm 0.06 \mu\text{g m}^{-3} \text{yr}^{-1}$) likely arises from overestimation of simulated summer time η values over the Eastern U.S.; both CALIPSO-adjusted and constant η values reduce anomalous features in the deseasonalized satellite-derived combined PM_{2.5} time series ($\pm 0.09 \mu\text{g m}^{-3} \text{yr}^{-1}$), however, fail to adequately account for trends in η . Comparison of trends inferred from satellite-derived PM_{2.5} to those from in situ measurements for other areas outside of the Eastern U.S. are depicted in SI Figure S5

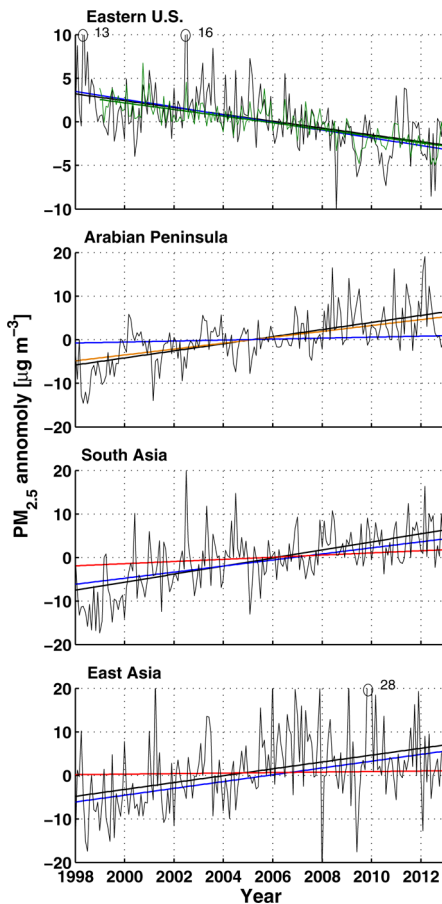


Figure 4. Regional monthly time series anomaly plots of satellite-derived PM_{2.5} from a combined MISR-SeaWiFS product and the corresponding modeled species attribution. Black indicates the satellite-derived time series and corresponding GLS linear fit. Other colors indicate the satellite-derived PM_{2.5} trend attributable to sulfate-nitrate-ammonium (blue), carbonaceous (red), and mineral dust (orange) aerosol as determined by the GEOS-Chem simulation. Green lines in the top panel are the in situ measured time series and corresponding GLS linear fit.

and presented in SI Table S1. The decrease in PM_{2.5} concentration over the U.S. occurring within this study period has been associated with increased life expectancy.²

Arabian Peninsula. Large increases in satellite-derived PM_{2.5} are apparent over the Arabian Peninsula. The regional time series anomaly has an increasing trend of $0.81 \pm 0.21 \mu\text{g m}^{-3} \text{ yr}^{-1}$. The increasing tendency occurs across all seasons,

with greater increases occurring for spring and summer months of the northern hemisphere—when low relative humidity, high temperature and high wind speeds facilitate dust mobilization from arid surfaces.⁴⁸ Positive trends in AOD from satellite^{15,21,23,49,50} and AERONET^{21,51} over a similar time period have been reported for this region. The GEOS-Chem simulation largely attributes the observed satellite-derived PM_{2.5} trend to changes in fine mineral dust. A decreasing Angstrom Exponent (a measure of increasing aerosol size) alongside positive AOD trends for this region provides further evidence of increasing dust load.^{21,51} Decreasing trends of dust emission from neighboring African deserts, with associated tropical Atlantic outflow, have been correlated with increases in North Atlantic sea surface temperature^{23,52} with suggestions of anthropogenic influence via a reduced indirect aerosol radiative forcing.⁵² Recent work has attributed the trends in dust emissions over the Arabian Peninsula to changes in wind speed and surface wetness²³ and associated these trends with local synoptic systems.⁵³ A much smaller increase in secondary inorganic and carbonaceous aerosol is also inferred from model attributed PM_{2.5} over this region. This increase is partially supported by satellite observations of increased tropospheric NO₂ over a similar period⁴⁶ that might have a causal relationship with aerosol nitrate formation or likely indicates increasing anthropogenic activities that contribute to primary and secondary particulate formation.

South Asia. Figure 3 shows large increases in satellite-derived PM_{2.5} over heavily populated regions of South Asia. Much of the Indo-Gangetic Basin experienced a statistically significant annual increase in PM_{2.5} of more than $1 \mu\text{g m}^{-3} \text{ yr}^{-1}$. The remaining landmass of South Asia, the Indian subcontinent in particular, has on average a statistically significant annual increase in PM_{2.5} of around $0.5 \mu\text{g m}^{-3} \text{ yr}^{-1}$. These spatial findings are in agreement with those reported by Dey et al.²⁸ for the Indian subcontinent over 2000–2010 despite their use of constant PM_{2.5} to AOD relationships—a result likely due to weak variation in South Asian η values over this period for much of the Indian subcontinent (SI Figure S3). The annual linear tendency for the South Asian region is $0.93 \pm 0.22 \mu\text{g m}^{-3} \text{ yr}^{-1}$. During the wet season (June–September), South Asia is influenced by strong monsoonal synoptic meteorology, during which time the Indian subcontinent can experience dust loads, especially heavy in the northern regions, from local (Thar) and neighboring (Arabian Peninsula) deserts.⁵⁴ The anomalous spring and summer low for the years 1998 and 1999 depicted in Figure 4 likely result from anomalously low dust outflow from these deserts as indicated from satellite-derived

Table 1. Annual Regional PM_{2.5} Trends over 1998–2012 and Corresponding 95% CI [$\mu\text{g m}^{-3} \text{ yr}^{-1}$] (as in Figure 4)

method	Eastern U.S. ^a	Eastern U.S.	Arabian Peninsula	South Asia	East Asia
temporal coverage [%] ^b	85	83	95	79	82
in situ	-0.38 ± 0.06	N/A	N/A	N/A	N/A
satellite-derived	-0.37 ± 0.13	-0.39 ± 0.10	0.81 ± 0.21	0.93 ± 0.22	0.79 ± 0.27
satellite-derived ^c	-0.22 ± 0.09	-0.23 ± 0.08	0.76 ± 0.19	0.78 ± 0.22	0.53 ± 0.23
model attributed PM _{2.5} ^d					
carbonaceous	0.04 ± 0.05	0	0.02 ± 0.01	0.25 ± 0.11	0.06 ± 0.16
secondary inorganic	-0.39 ± 0.11	-0.39 ± 0.10	0.11 ± 0.08	0.70 ± 0.19	0.78 ± 0.27
fine mineral dust	0	0	0.68 ± 0.19	-0.04 ± 0.23	-0.04 ± 0.18

^aTrends inferred over 1999–2012, a period of available in situ measurements. ^bAverage grid box temporal coverage within region after 65% threshold was applied prior to trend inference—see SI Figure S2 for global map of temporal coverage. ^cSatellite-derived calculated with constant η .

^dCalculated from the satellite-derived PM_{2.5} time series scaled by the fractional GEOS-Chem PM_{2.5} components.

$\text{PM}_{2.5}$ concentrations in dust outflow affected regions for these two years (data not shown). From October–February, South Asia is under very different synoptic meteorology which can favor the regional buildup of anthropogenic aerosols.^{28,54,55} Our modeled species attribution to the observed annual South Asian trend consists of statistically significant increases in secondary inorganic and carbonaceous aerosols. Rising power sector coal consumption without flue gas desulfurization is largely responsible for the steady increases in sulfur dioxide emissions across South Asia over the past decade.⁵⁶ Emissions of carbonaceous aerosols continue to increase over South Asia, largely following residential biofuel use and energy consumption.⁵⁷

East Asia. For the period 1998–2012, East Asia has the highest annual average surface burden of satellite-derived $\text{PM}_{2.5}$ in the world. Erratic seasonal variation is observed in the monthly time series which displays fluctuating summer and winter enhancements. Summer enhancements in secondary inorganics are due to favorable oxidation pathways and winter enhancements in the carbonaceous component are due to dry-stable conditions with large anthropogenic emissions.⁵⁸ An increase of $0.79 \pm 0.27 \mu\text{g m}^{-3} \text{ yr}^{-1}$ in $\text{PM}_{2.5}$ was observed which GEOS-Chem mostly attributes to large increases in secondary inorganic aerosols ($0.78 \pm 0.27 \mu\text{g m}^{-3} \text{ yr}^{-1}$). The East Asian time series steadily increases until 2007 then levels off. Xu et al.⁵⁹ describe abatement incentives in China since 2007 where installation and increased use of flue gas desulfurization systems occurred in coal fired power plants. Meanwhile, industrial sector emissions continue to increase.^{56,57} As seen in Figure 3, local hotspots of significant increase in East Asia appear south of Beijing and throughout inland floodplains to the Pearl River Delta, which match well the temporally resolved emission distributions of primary and secondary anthropogenic particulate sources throughout this region.^{46,57} Recent studies examining the long-term trend in manually estimated atmospheric visibility, which is nonlinearly sensitive to $\text{PM}_{2.5}$ as well as meteorological conditions such as relative humidity, offer a qualitative proxy to the trend in surface $\text{PM}_{2.5}$.⁶⁰ Several long-term visibility studies over various regions in China exhibit the “leveling off” feature observed in Figure 4 for East Asia, where degrading annual average visibility stabilizes or begins to improve after 2006.^{61–64}

Overall, the 15-year unified MISR- and SeaWiFS-derived global $\text{PM}_{2.5}$ monthly time series is consistent with the corresponding linear tendency observed from in situ observations over the Eastern U.S. and with current understanding elsewhere. Time varying “ $\text{PM}_{2.5}$ to AOD” relationships were necessary to reproduce the trends in in situ observations. An emerging global surface particulate matter network (SPARTAN, <http://www.spartan-network.org/>) collocated with AERONET sites will offer further information to understand “ $\text{PM}_{2.5}$ to AOD” relationships over a variety of regions.⁶⁵ Our effort developed the time series of $\text{PM}_{2.5}$ anomalies over 1998–2012; van Donkelaar et al. (submitted)⁶⁶ extend this work by combining these anomalies with other existing absolute satellite-derived $\text{PM}_{2.5}$ estimates from two data sets spanning the first⁶ and second³⁸ half of the 1998–2012 study period for comparison with World Health Organization air quality guidelines. Future effort would benefit from the improved spatiotemporal coverage resulting from incorporation of both MODIS-Terra and –Aqua AOD sensors from the radiometric stabilized collection 6 data set.

ASSOCIATED CONTENT

Supporting Information

Contained in the Supporting Information for this article is a detailed description of the GEOS-Chem chemical transport model and how it was used in this study. In addition, five supplemental figures and one table are included. This material is available free of charge via the Internet at <http://pubs.acs.org/>.

AUTHOR INFORMATION

Corresponding Author

*Phone: +19024941820; fax: +19024941123; e-mail: briboys@gmail.com.

Notes

The authors declare no competing financial interest.

ACKNOWLEDGMENTS

Funding for this work was provided by NSERC Canada and by an Izaak Walton Killiam Memorial Scholarship for B. L. Boys. Computational facilities are partially provided by ACEnet, the regional high performance computing consortium for universities in Atlantic Canada. We thank the AERONET, MISR, SeaWiFS, CALIPSO, IMPROVE, and AQS science teams for making their data publicly available.

REFERENCES

- (1) Dockery, D.; Pope, C. A. I.; Xu, X.; Spengler, J. D.; Ware, J. H.; Fay, M. E.; Ferris, G.; Speizer, F. E. An association between air pollution and mortality in six U.S. cities. *N. Engl. J. Med.* **1993**, *329*, 1753–1759.
- (2) Correia, A. W.; Pope, C. A. I.; Dockery, D.; Wang, Y.; Ezzati, M.; Dominici, F. An analysis of 545 U.S. counties for the period from 2000 to 2007. *Epidemiology* **2013**, *24*, 23–31.
- (3) Lim, S. S.; Vos, T.; Flaxman, A. D.; Danaei, G.; Shibuya, K.; Adair-Rohani, H.; AlMazroa, M.; et al. A comparative risk assessment of burden of disease and injury attributable to 67 risk factors and risk factor clusters in 21 regions, 1990–2010: A systematic analysis for the Global Burden of Disease Study 2010. *Lancet* **2012**, *380*, 2224–2260.
- (4) Pedersen, M.; Giorgis-Allemand, L.; Bernard, C.; Aguilera, I.; Andersen, A.; Ballester, F.; Beelen, R.; et al. Ambient air pollution and low birthweight: A European cohort study (ESCAPE). *Lancet* **2013**, DOI: 10.1016/s2213-2600(13)70192-9.
- (5) IARC. *Outdoor Air Pollution a Leading Environmental Cause of Cancer Deaths*; WHO, 2013; Vol. N221.
- (6) van Donkelaar, A.; Martin, R. V.; Brauer, M.; Kahn, R.; Levy, R.; Verduzco, C.; Villeneuve, P. J. Global estimates of ambient fine particulate matter concentrations from satellite-based aerosol optical depth: Development and application. *Environ. Health Perspect.* **2010**, *847*–855.
- (7) Crouse, D. L.; Peters, P. A.; van Donkelaar, A.; Goldberg, M. S.; Villeneuve, P. J.; Brion, O.; Khan, S.; Atario, D. O.; Jerrett, M.; Pope, C. A.; et al. Risk of nonaccidental and cardiovascular mortality in relation to long-term exposure to low concentrations of fine particulate matter: A Canadian national-level cohort study. *Environ. Health Perspect.* **2012**, *120*, 708–714.
- (8) Engel-Cox, J.; Oanh, N. T. K.; van Donkelaar, A.; Martin, R. V. Toward the next generation of air quality monitoring: Particulate Matter. *Atmos. Environ.* **2013**, *80*, 584–590.
- (9) Liu, Y.; Park, R. J.; Jacob, D. J.; Li, Q. Mapping annual mean ground-level $\text{PM}_{2.5}$ concentrations using multiangle imaging spectroradiometer aerosol optical thickness over the contiguous United States. *J. Geophys. Res.* **2004**, *109*, D22206.
- (10) Hu, X.; Waller, L. A.; Lyapustin, A.; Wang, Y.; Liu, Y. 10 yr spatial and temporal trends of $\text{PM}_{2.5}$ concentrations in the southeastern US estimated using high-resolution satellite data. *Atmos. Chem. Phys.* **2013**, *14*, 6301–6314.

- (11) Lee, H. J.; Liu, Y.; Coull, B. A.; Schwartz, J.; Koutrakis, P. A novel calibration approach of MODIS AOD data to predict PM_{2.5} concentrations. *Atmos. Chem. Phys.* **2011**, *11*, 7991–8002.
- (12) Li, Z.; Zhao, X.; Kahn, R.; Mishchenko, M.; Remer, L.; Lee, K. H.; Wang, M.; Laszlo, I.; Nakajima, T.; Maring, H. Uncertainties in satellite remote sensing of aerosols and impact on monitoring its long-term trend: A review and perspective. *Ann. Geophys.* **2009**, *27*, 2755–2770.
- (13) Colarco, P. R.; Kahn, R. A.; Remer, L. A.; Levy, R. C. Impact of satellite viewing swath width on global and regional aerosol optical thickness statistics and trends. *Atmos. Meas. Technol. Discuss.* **2013**, *6*, 10117–10163.
- (14) Zhao, X.; Laszlo, I.; Guo, W.; Heidinger, A.; Cao, C.; Jelenak, A.; Tarpley, D.; Sullivan, J. Study of long-term trend in aerosol optical thickness observed from operational AVHRR satellite instrument. *J. Geophys. Res.* **2008**, *113*, D07201.
- (15) Zhang, J.; Reid, J. S. A decadal regional and global trend analysis of the aerosol optical depth using a data-assimilation grade over-water MODIS and Level 2 MISR aerosol products. *Atmos. Chem. Phys.* **2010**, *10* (22), 10949–10963, DOI: 10.5194/acp-10-10949-2010.
- (16) Levy, R. C.; Mattoe, S.; Munchak, L. A.; Remer, L. A.; Sayer, A. M.; Patadia, F.; Hsu, N. C. The collection 6 MODIS aerosol products over land and ocean. *Atmos. Meas. Tech.* **2013**, *6* (11), 2989–3034, DOI: 10.5194/amt-6-2989-2013.
- (17) Barnes, R. A.; Eplee, R. E.; Schmidt, M.; Patt, F. S.; McClain, C. R. Calibration of SeaWiFS, I: Direct techniques. *Appl. Opt.* **2001**, *40*, 6682–6700.
- (18) Eplee, R. E.; Meister, G.; Patt, F. S.; Barnes, R. A.; Bailey, S. W.; Franz, B. A.; McClain, C. R. On-orbit calibration of SeaWiFS. *Appl. Opt.* **2012**, *51*, 8702–8730.
- (19) Bruegge, C. J.; Diner, D. J.; Kahn, R. A.; Chrien, N.; Helminger, M. C.; Gaitley, B. J.; Abdou, W. A. The MISR radiometric calibration process. *Rem. Sens. Environ.* **2007**, *107*, 2–11.
- (20) Kahn, R.; Li, W. H.; Martonchik, J. V.; Bruegge, C. J.; Diner, D.; Gaitley, B. J.; Abdou, W.; Dubovik, O.; Holben, B.; Smirnov, A.; Jin, Z.; Clark, D. MISR calibrations and implications for low-light-level aerosol retrieval over dark water. *J. Atmos. Sci.* **2005**, *62*, 1032–1062.
- (21) Hsu, C.; Gautam, R.; Sayer, A. M.; Bettenhausen, C.; Li, C.; Jeong, M. J.; Tsay, S. C.; Holben, B. N. Global and regional trends of aerosol optical depth over land and ocean using SeaWiFS measurements from 1997 to 2010. *Atmos. Chem. Phys.* **2012**, *12*, 8037–8053.
- (22) Yoon, J.; von Hoyningen-Huene, W.; Vountas, M.; Burrows, J. P. Analysis of linear long-term trend of aerosol optical thickness derived from SeaWiFS using BAER over Europe and South China. *Atmos. Chem. Phys.* **2011**, *11*, 12149–12167.
- (23) Chin, M.; Diehl, T.; Tan, Q.; Prospero, J. M.; Kahn, R. A.; Remer, L. A.; Yu, H.; Sayer, A. M.; Bian, H.; Geogdzhayev, I. V.; Holben, B. N.; Howell, S. G.; et al. Multi-decadal aerosol variations from 1980 to 2009: A perspective from observations and a global model. *Atmos. Chem. Phys.* **2014**, *14*, 3657–3690.
- (24) Wang, K.; Dickinson, R. E.; Liang, S. Clear sky visibility has decreased over land globally from 1973 to 2007. *Science* **2009**, *323*, 1468–1470.
- (25) Berglen, T. F.; Myhre, G.; Isaksen, I. S. A.; Vestreng, V.; Smith, S. J. Sulphate trends in Europe: Are we able to model the recent observed decrease? *Tellus* **2007**, *59*, 773–786.
- (26) Cheng, Z.; Jiang, J.; Fajardo, O.; Wang, S.; Hao, J. Characteristics and health impacts of particulate matter pollution in China (2001–2011). *Atmos. Environ.* **2013**, *65*, 186–194.
- (27) Wang, K. C.; Dickinson, R. E.; Trenberth, K. E. Contrasting trends of mass and optical properties of aerosols over the Northern Hemisphere from 1992 to 2011. *Atmos. Chem. Phys.* **2012**, *12*, 9387–9398.
- (28) Dey, S.; Di Girolamo, L.; van Donkelaar, A.; Tripathi, S. N.; Gupta, T.; Mohan, M. Variability of outdoor fine particulate (PM_{2.5}) concentration in the Indian Subcontinent: A remote sensing approach. *Rem. Sens. Environ.* **2012**, *127*, 153–161.
- (29) Diner, D. J.; Beckert, J. C.; Reilly, T. H.; Bruegge, C. J. Multi-angle imaging spectroradiometer (MISR) instrument description and experiment overview. *IEEE Trans. Geosci. Remote Sens.* **1998**, *36* (4), 1072–1087.
- (30) Martonchik, J. V.; Diner, D. J.; Kahn, R. A.; Ackerman, T. P.; Verstraete, M. M.; Pinty, B.; Gordon, H. R. Techniques for the retrieval of aerosol properties over land and ocean using multiangle imaging. *IEEE Trans. Geosci. Remote Sens.* **1998**, *36*, 1212–1226.
- (31) Martonchik, J. V.; Diner, D. J.; Kahn, R.; Gaitley, B. Comparison of MISR and AERONET aerosol optical depths over desert sites. *Geophys. Res. Lett.* **2004**, *31*, L16102.
- (32) Sayer, A. M.; Hsu, N. C.; Bettenhausen, C.; Ahmad, Z.; Holben, B. N.; Smirnov, A.; Thomas, G. E.; Zhang, J. SeaWiFS ocean aerosol retrieval (SOAR): Algorithm, validation, and comparison with other data sets. *J. Geophys. Res.* **2012**, *117*, D03206.
- (33) Hsu, N. C.; Jeong, M. J.; Bettenhausen, C.; Sayer, A. M.; Hansell, R.; Seftor, C. S.; Huang, J.; Tsay, S.-. Enhanced deep blue aerosol retrieval algorithm: The second generation. *J. Geophys. Res.* **2013**, *118*, 1–20.
- (34) Petenko, M.; Ichoku, C. Coherent uncertainty analysis of aerosol measurements from multiple satellite sensors. *Atmos. Chem. Phys.* **2013**, *13*, 6777–6805.
- (35) Reference Method for the Determination of Fine Particulate Matter as PM_{2.5} in the Atmosphere, 40CFR50; U.S. Environmental Protection Agency, 1997; Appendix L.
- (36) Bey, I.; Jacob, D. J.; Yantosca, R. M.; et al. Global modeling of tropospheric chemistry with assimilated meteorology: Model description and evaluation. *J. Geophys. Res.* **2001**, *106*, 23073–23095.
- (37) Park, R. J.; Jacob, D. J.; Field, B. D.; Yantosca, R. M. Natural and transboundary pollution influences on sulfate-nitrate-ammonium aerosols in the United States: Implications for policy. *J. Geophys. Res.* **2004**, *109*, 1029/2003JD004473.
- (38) van Donkelaar, A.; Martin, R. V.; Spurr, R. J. D.; Drury, E.; Remer, L. A.; Levy, R. C.; Wang, J. Optimal estimation for global ground-level fine particulate matter concentrations. *J. Geophys. Res.* **2013**, *118*, 10.1002/jgrd.50479.
- (39) Lee, H. J.; Liu, Y.; Coull, B. A.; Schwartz, J.; Koutrakis, P. A novel calibration approach of MODIS AOD data to predict PM_{2.5} concentrations. *Atmos. Chem. Phys.* **2011**, *11*, 7991–8002.
- (40) Levy, R.; Leptoukh, G.; Kahn, R.; Zubko, V.; Gopalan, A.; Remer, L. A critical look at deriving monthly aerosol optical depth from satellite data. *IEEE Trans. Geosci. Remote Sens.* **2009**, *47* (8), 2942–2956.
- (41) Shumway, R. H.; Stoffer, D. S. *Time Series Analysis and Its Applications*, 3rd ed.; Springer, 2011.
- (42) Weatherhead, E. C.; Reinsel, G. C.; Tiao, G. C.; Meng, X.-.; Choi, D.; Cheang, W.-.; Keller, T.; DeLuisi, J.; Ruebbles, D. J.; Kerr, J. B.; Miller, A. J.; Oltmans, S. J.; Frederick, J. E. Factors affecting the detection of trends: Statistical considerations and applications to environmental data. *J. Geophys. Res.* **1998**, *103*, 17149–17161.
- (43) Weatherhead, E. C.; Stevermer, A. J.; Schwartz, B. E. Detecting environmental changes and trends. *Phys. Chem. Earth, C* **2002**, *27*, 399–403.
- (44) Duncan, B. N.; Martin, R. V.; Staudt, A. C.; Yevich, R.; Logan, J. A. Interannual and seasonal variability of biomass burning emissions constrained by satellite observations. *J. Geophys. Res.* **2003**, *108*; 10.1029/2002JD002378.
- (45) Koren, I.; Remer, L. A.; Longo, K. Reversal of trend of biomass burning in the Amazon. *Geophys. Res. Lett.* **2007**, *34*, L20404.
- (46) Hilboll, A.; Richter, A.; Burrows, J. P. Long-term changes of tropospheric NO₂ over megacities derived from multiple satellite instruments. *Atmos. Chem. Phys.* **2013**, *13*, 4145.
- (47) Leibensperger, E. M.; Mickley, L. J.; Jacob, D. J.; Chen, W.-.; Seinfeld, J. H.; Nenes, A.; Adams, P. J.; Streets, D. G.; Kumar, N.; Rind, D. Climatic effects of 1950–2050 changes in US anthropogenic aerosols—Part 1: Aerosol trends and radiative forcing. *Atmos. Chem. Phys.* **2012**, *12*, 3333–3348.
- (48) Shahsavani, A.; Naddafi, K.; Haghifard, N. J.; Mesdaghinia, A.; Yunesian, M.; Nabizadeh, R.; Arahami, M.; Sowlat, M. H.; Yarahmadi, M.; Saki, H.; et al. The evaluation of PM₁₀, PM_{2.5}, and PM₁ concentrations during the Middle Eastern Dust (MED) events in

Ahvax, Iran, from April through September 2010. *J. Arid Environ.* **2012**, *77*, 72–83.

(49) de Meij, A.; Pozzer, A.; Lelieveld, J. Trend analysis in aerosol optical depths and pollutant emission estimates between 2000 and 2009. *Atmos. Environ.* **2012**, *51*, 75–85.

(50) Murphy, D. M. Little net clear-sky radiative forcing from recent regional redistribution of aerosols. *Nat. Geosci.* **2013**, *6*, 258–262.

(51) Yoon, J.; von Hoyningen-Huene; Kokhanovsky, A. A.; Vountas, M.; Burrows, J. P. Trend analysis of aerosol optical thickness and Angstrom exponent derived from the global AERONET spectral observations. *Atmos. Meas. Technol.* **2012**, *5*, 1271–1299.

(52) Ridley, D. A.; Heald, C. L.; Prospero, J. M. What controls the recent changes in African mineral dust aerosol across the Atlantic? *Atmos. Chem. Phys.* **2014**, *14*, 5735–5747.

(53) Ganor, E.; Osetinskey, I.; Stupp, A.; Alpert, P. Increasing trend of African dust, over 49 years in the eastern Mediterranean. *J. Geophys. Res.* **2010**, *115*, D07201.

(54) Sagnik, D.; Di Girolamo, L. A climatology of aerosol optical and microphysical properties over the Indian subcontinent from 9 years (2000–2008) of Multiangle Imaging Spectroradiometer (MISR) data. *J. Geophys. Res.* **2010**, *115*, D15204.

(55) Dey, S.; Girolamo, D. L. A decade of change in aerosol properties over the Indian subcontinent. *Geophys. Res. Lett.* **2011**, *38*, L14811.

(56) Klimont, K.; Smith, S. J.; Cofala, J. The last decade of global anthropogenic sulfur dioxide: 2000–2011 emissions. *Environ. Res. Lett.* **2013**, *8*, 014003.

(57) Lu, Z.; Zhang, Q.; Streets, D. G. Sulfur dioxide and primary carbonaceous aerosol emissions in China and India, 1996–2010. *Atmos. Chem. Phys.* **2011**, *11*, 9839–9864.

(58) Zhang, R.; Jing, P.; Tao, J.; Hsu, S.-.; Wang, G.; Cao, J.; Lee, C. S. L.; Zhu, L.; Chen, Z.; Zhao, Y.; Shen, Z. Chemical characterization and source apportionment of PM_{2.5} in Beijing: Seasonal perspective. *Atmos. Chem. Phys.* **2013**, *13*, 7053–7074.

(59) Xu, Y. Improvements in the operation of SO₂ Scrubbers in China's coal power plants. *Environ. Sci. Technol.* **2011**, *45*, 380–385.

(60) Deng, X.; Tie, X.; Wu, D.; Xhou, X.; Bi, X.; Tan, H.; Li, F.; Jiang, C. Long-term trend of visibility and its characterizations in the Pearl River Delta (PRD) region, China. *Atmos. Environ.* **2008**, *42*, 1424–1435.

(61) Cheng, Z.; Wang, S.; Jiang, J.; Fu, Q.; Chen, C.; Xu, B.; Yu, J.; Fu, X.; Hao, J. Long-term trend of haze pollution and impact of particulate matter in the Yangtze River Delta, China. *Environ. Pollut.* **2013**, *182*, 101–110.

(62) Deng, J.; Du, K.; Wang, K.; Yuan, C.-.; Zhao, J. Long-term atmospheric visibility trend in Southeast China, 1973–2010. *Atmos. Environ.* **2012**, *59*, 11–21.

(63) Chen, Y.; Xie, S. Long-term trends and characteristics of visibility in two megacities in southwest China: Chengdu and Chongqing. *J. Air Waste Manage. Assoc.* **2013**, *63*, 1058–1069.

(64) Zhao, P.; Zhang, X.; Xu, X.; Zhao, X. Long-term visibility trends and characteristics in the region of Beijing, Tianjin, and Hebei, China. *Atmos. Res.* **2011**, *101*, 711–718.

(65) Snider, G.; Weagle, C. L.; Martin, R. V.; van Donkelaar, A.; Conrad, K.; Zwicker, M.; Akoshile, C.; Artaxo, P.; Anth, N. X.; Brook, J.; et al. SPARTAN: A global network to evaluate and enhance satellite-based estimates of ground-level particulate matter for global health applications. *Atmos. Meas. Technol. Discuss.* **2014**, *7*, 7569–7611.

(66) van Donkelaar, A.; Martin, R. V.; Brauer, M.; Boys, B. L. Global fine particulate matter concentrations from satellite for long-term exposure assessment. *Environ. Health Perspect.* **2014**, submitted.